

Density Fluctuation of GAM Zonal Flows on the HL-2A Tokamak

L. W. Yan 1), J. Cheng 1), K. J. Zhao 1), J. Q. Dong 1), W. Y. Hong 1), J. Qian 1),
X. M. Song 1), Q. W. Yang 1), X. R. Duan 1), C. H. Pan 1) , Y. Liu 1)

1) Southwestern Institute of Physics, P. O. Box 432, Chengdu 610041, China
E-mail contact of main author: lwyan@swip.ac.cn

Abstract. The density fluctuation of Geodesic Acoustic Mode (GAM) zonal flow has been observed in Ohmic deuterium plasma discharges with Langmuir probe arrays on the HL-2A tokamak. The density fluctuation has the poloidal mode number $m < 1$ and toroidal mode number $n \sim 0$. Its amplitude is consistent with theoretic prediction as well. Bispectral analysis shows that the nonlinear interaction between the GAM zonal flow and high frequency ambient turbulence (HFAT) is a plausible mechanism for the generation of the GAM. The phase shifts between the GAM and its envelope of the HFAT (200-450 kHz) with different poloidally separations are $\pi/2$ to π , indicating that the ambient turbulence is regulated by the GAM through envelope modulation.

Keyword: Zonal flow, fluctuations, long range correlation, potential turbulence, turbulence studies

1. Introduction

Turbulence theory predicts the transport is strongly affected by the existence of self-generated zonal flow (ZF) [1-2]. Therefore, the investigation of the ZF and the nonlinear coupling between it and ambient turbulence becomes a hot topic in toroidal plasmas [3-5]. The zonal flow has two branches: one is called low frequency zonal flow (LFZF) and the other is higher frequency zonal flow, named as GAM Zonal Flow (GAMZF) existing in potential and density fluctuations. The GAMZF is driven by ambient turbulence, and then can regulate the ambient turbulence, in turn. The characteristics of GAM potential fluctuations have been widely explored in various plasma experiments [6-10]. The poloidal symmetry of GAM structure in potential fluctuations was identified as $m \sim 0$ in JIPPT-IIU [11], JFT-2M [12] and T-10 [13]. The modulation process, linked to the generation of zonal flows by the HFAT and significant nonlinear coupling between the GAM and ambient turbulence, has already been confirmed in potential fluctuations with bispectral analysis [14-16]. The poloidal and toroidal symmetries ($m = n = 0$) of GAM potential fluctuations have also been verified with a novel probe arrays on the HL-2A tokomak [17-19]. Recently, the LFZF has been observed in DIII-D with beam emission spectroscopy [20] and in HL-2A with Langmuir probe (LP) arrays [21]. Because the GAM fluctuation is that the $m = n = 0$ electrostatic potential is linearly coupled to the $m = 1, n = 0$ sideband density fluctuation [2], it is observed that the GAM density fluctuations have poloidal number $m \approx 10$ at $r/a = 0.90$ in DIII-D [6] with beam emission spectroscopy, and $m = 0$ at $r/a = 0.93$ in T-10 with correlation reflectometer [22]. On TEXTOR, there is a report about the poloidal asymmetry of GAM amplitude in density fluctuations between midplane and top positions [22], which is consistent with the theoretical prediction ($m = 1$). So far, however, the toroidal mode number ($n = 0$) and

the comprehensive spectral characteristics of GAM density fluctuations have not been discussed yet. Especially, there is lack of sufficient experimental evidence to confirm the nonlinear coupling between the GAMZF and the ambient turbulence in density fluctuations, though it is identified in potential fluctuations.

In this paper, the poloidal asymmetry, toroidal symmetry, and the nonlinear coupling mechanism for the GAM density fluctuations, are investigated with the LP arrays inside the last closed flux surface (LCFS). The toroidal mode number ($n = 0$) and amplitude of GAM density fluctuations are consistent with theoretical prediction. The nonlinear coupling between the GAMZF and the HFAT is confirmed with bispectral and envelope analysis.

This paper is arranged as follows. Part 2 introduces the data analysis methods for the GAMZF. Part 3 describes the experimental setup. The experimental results are presented in part 4. Part 5 is for the summary.

2. Data analysis methods

2.1. Bispectrum analysis

Bispectrum analysis [23] consists in calculating three-cumulated spectrum defined as

$$B(f_1, f_2) = \langle X(f_1)Y(f_2)Z^*(f_3 = f_1 \pm f_2) \rangle, \quad (1)$$

where $X(f)$, $Y(f)$ and $Z(f)$ are the Fourier components of the time traces of $x(t)$, $y(t)$ and $z(t)$, respectively; the symbol $\langle \rangle$ denotes ensemble averaging over many realizations. Three-wave interaction occurs under the condition of $k_3 = k_1 \pm k_2$ and $f_3 = f_1 \pm f_2$, where k_j and f_j

$(j = 1, 2, 3)$ are wave-numbers and frequencies of the three waves, respectively. The squared bicoherence is defined as,

$$b^2(f_1, f_2) = \frac{|B(f_1, f_2)|^2}{\langle |X(f_1)Y(f_2)|^2 \rangle \langle Z(f_3)Z^*(f_3) \rangle} \quad (2)$$

with $0 \leq b^2(f_1, f_2) \leq 1$. The summation of squared bicoherence is used to denote total contribution of nonlinear three-wave coupling to a Fourier component, which specifies the nonlinear coupling from many modes to a mode. It is defined as

$$b_s^2(f = f_1 \pm f_2) = \sum_{i=1}^N b_i^2(f_1 + f_2)/N. \quad (3)$$

The phase angle of three-wave interaction is given by the biphase, which is a phase angle of the complex $B(f_1, f_2)$, defined as $\theta = \arctan \frac{\text{Im } B(f_1, f_2)}{\text{Re } B(f_1, f_2)}$. In order to more exactly investigate the

three-wave coupling, it is important to obtain the bispectral function that is much larger than noise level, which has the value of $(1-b^2)/M$, where M is the number of realizations and $b^2 \ll 1$.

Therefore, the noise level will decrease to zero if the $M \rightarrow \infty$. The best method to improve the signal to noise ratio and to clarify mainly nonlinear coupling is using a large M.

2.2. Envelope analysis

The modulation interaction among three waves can be characterized with envelope analysis [24]. To obtain the envelope from the original signals in finite frequency band, firstly a filtering process to the original signals needs carrying out. Then the Hilbert transform for the filtered signals $S_f(t)$ is executed to obtain the analytic signal $H(t)$, defined as $H(t)=S_f(t)+iH_f(t)$, where $H_f(t)$ is the Hilbert transform of the $S_f(t)$, whose complex phase angle is shifted by $\pi/2$,

$$H_f(t) = \frac{1}{\pi} \int_{-\infty}^{\infty} \frac{S_f(t')}{t - t'} dt'. \quad (4)$$

The envelope is defined as the analysis coefficient of the analytic signal $H(t)$. The information on the nonlinear interaction is embodied in the envelope. Thus, the modulation interaction can be identified with cross correlation technique.

3. Experimental setup

HL-2A is a medium-sized tokamak with $R = 1.65$ m and $a = 0.40$ m. The present experiment is carried out in Ohmic deuterium discharges with $B_t = 1.4$ T, $I_p = 180$ kA, $n_e = 1.6 \times 10^{13}$ cm $^{-3}$, $q_a \sim 3.5$. Typical discharge duration is about 1500 ms. Main diagnostics in the experiment are the LP arrays located at the outer midplane [25, 26]. Recently, a novel design combined rake probes with three-step Langmuir probes (TSLPs) is used to measure the GAM density fluctuation on HL-2A, as shown in Fig. 1. The rake probe array consists of 10 tips with the diameter of 1.5 mm and height of 2 mm, the adjacent and largest separations of 4 mm and 36 mm. The TSLP array is applied to measure the radial coherence. Both probe arrays have a toroidal span of ~ 1.33 m or an angle of 37.5° . They are used to determine the poloidal and toroidal mode numbers of the GAMZF simultaneously. Each tip as single probe measures the saturation ion current (I_s). The fast Fourier transform (FFT), bispectrum technique and envelope analysis are applied to the data analysis with the duration of 200 ms. The data from LPs are digitized at the frequency $f_s = 1$ MHz of 12 bit accuracy, corresponding Nyquist frequency of the FFT analysis is $f_N = f_s/2 = 500$ kHz.

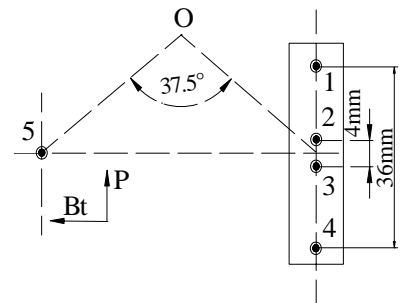


FIG. 1. Schematic arrangement of two probe arrays with 5 tips

4. Experimental results

4.1. Spectral characteristics of density fluctuations with the GAM frequency

The relative density fluctuation is replaced by the relative I_s fluctuation because the relative temperature fluctuation contributes smaller than <10% [27]. The power spectra are

obtained by an FFT of 1024 points (0.98 kHz frequency resolution) with 50% overlapping of Hanning window. Subtraction of the linear trend and multiplication by the window functions are performed prior to the FFT. The auto power spectra (APS) of the density and potential fluctuations in shot 8847 are shown in Figs. 2(a) and 2(b). There are three peaks in the APS. The first peak at the 2.5 kHz is clear in Fig. 2(a), but it is ambiguous in Fig. 2(b), corresponding to the LFZF [21]. The second appears in the density and potential spectra with a frequency of 9.8 kHz, consistent with the frequency predicted by the GAM theory [2, 28],

$$f_{\text{GAM,th}} = ((T_i + T_e)/M_i)^{1/2}/(2\pi R)(1+1/(2q^2)) = 9.0 \text{ kHz},$$

where M_i is the ion mass, T_i is assumed to equal T_e , and $T_e = 48 \text{ eV}$ is local electron temperature measured at $r/a=0.95$. The full width at half magnitude (FWHM) of the density fluctuation is $\Delta f = 3.9 \text{ kHz}$, corresponding lifetime is $\sim 256 \mu\text{s}$. The relative amplitude of the GAM density fluctuation near outer midplane is estimated as 0.02% with the HFAT envelope amplitude $\tilde{n}_{\text{GAM}}^{\text{env}} / \tilde{n}_e = 0.4\%$ in 100-450 kHz multiplying total density fluctuation $\tilde{n}_e / \bar{n}_e = 5\%$, while it is predicted as $\tilde{n}_{\text{GAM}}^{\text{the}} / n_e = -\sqrt{2}k_r\rho_i(e\tilde{\phi}/T_e)\sin\theta = 0.03\%$ by the GAM theory using the following parameters: $k_r\rho_i = 0.07$, $e\tilde{\phi}/T_e = 6.2\%$, and $\theta = 2.7^\circ$. Both theoretical and experimental amplitudes are in qualitative agreement. The last peak in density spectrum with wide frequency range in 20-80 kHz is labeled as quasi-coherent mode of ambient turbulence [29]. The coherency between I_s and V_f is shown in Fig. 2(c). The coherency at the GAM frequency reaches 0.8, which is higher than that of broadband fluctuations in 20-80 kHz. The phase shift at GAM frequency given in Fig. 2(d) is about 0.45π , close to theoretical prediction of 0.5π .

Using the two-point correlation technique [19], the local mode number-frequency spectra for I_s fluctuations, i.e., $S(m,f)$ and $S(n,f)$, have been estimated. Tips 1 and 4 are used to evaluate poloidal mode number m , while tips 2 and 5 for toroidal mode number n , i.e. $m = k_\theta d_\theta/\theta_{14}$, $n = k_\phi d_\phi/\Phi_{25}$, where d_θ is poloidal distance, θ_{14} is the poloidal angle between tips 1 and 4. The Contour plots of $S(m,f)$ and $S(n,f)$ are shown in Fig. 3. It is clear that the

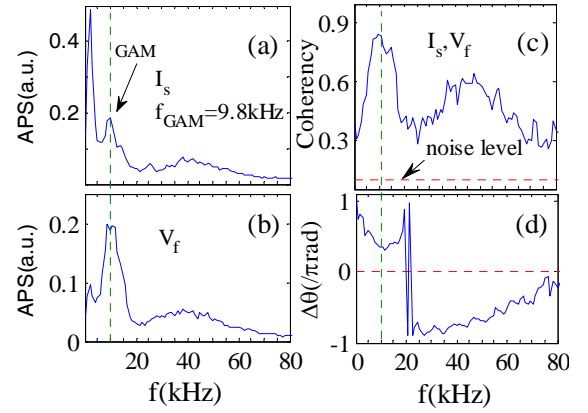


FIG. 2. Auto power spectra of I_s (a) and V_f (b), coherence between I_s and V_f (c), corresponding phase shift spectra (d).

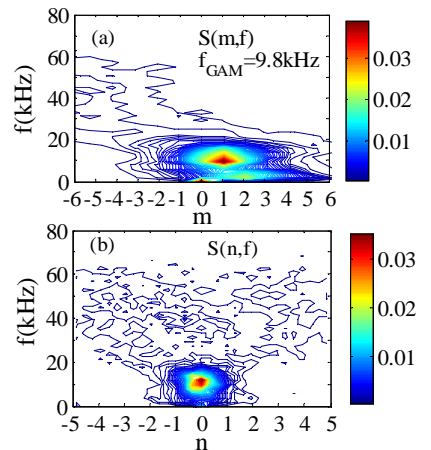


FIG. 3. Mode number-frequency spectra $S(m,f)$ and $S(n,f)$ of I_s fluctuations.

spectrum $S(m,f)$ concentrates in the region of $9 < f < 13$ kHz and $0 < m < 2$. The ambient density turbulence is observed to propagate in the electron diamagnetic direction in the frequency range of $20 < f < 60$ kHz with mode number $-6 < m < -2$, as shown in Fig. 3(a). The slope of the frequency f versus the wave vector ($k \sim m$) denotes the poloidal velocity. Toroidal mode number is estimated with the same method, as shown in Fig. 3(b). The GAM spectrum $S(n,f)$ appears in the region of $9 < f < 13$ kHz and $0 < n < 0.2$. The spectral averaged wave-number k_m and its width Δk for I_s fluctuations has been evaluated from the spectrum $S(k,f)$, i.e., $k = k_m \pm \Delta k$. The poloidal and toroidal wave numbers are estimated to be $k_\theta = (3.5 \pm 1.6) \times 10^{-2}$ cm $^{-1}$ and $k_\varphi = (2 \pm 3) \times 10^{-4}$ cm $^{-1}$, the corresponding poloidal and toroidal mode numbers are $m = 1.2 \pm 0.4$ and $n = 0.036 \pm 0.039$. In another discharge without potential measurement, the mode numbers of the GAM density fluctuations are given as $m = -0.73 \pm 0.65$ and $n = 0.035 \pm 0.04$. Similarly, the mode numbers for the GAM potential fluctuations are $m = 0.23 \pm 0.36$ and $n = 0.04 \pm 0.04$.

4.2. Bispectral analysis of generation mechanism of GAM density fluctuation

It has been predicted that the ZF energy originates from the three-wave coupling of ambient turbulence. This energy cascade process can be observed with bispectral analysis. The squared bicoherence $b^2(f_1, f_2)$, an indicator of nonlinear coupling, is calculated with the frequency resolution of $\Delta f = 0.98$ kHz. Figure 4(a) shows the squared auto-bicoherence of I_s , which is plotted in the region between the lines of the $f_1 - f_2 = 0$ and $f_1 + f_2 = 0$ in the $f_1 - f_2$ plane. Positive and negative f_2 mean the regions of the $f = f_1 + |f_2|$ and $f = f_1 - |f_2|$, respectively. The graph is symmetric with respect to the line $f_1 - f_2 = 0$ ($f_2 > 0$) and the line $f_1 + f_2 = 0$ ($f_2 < 0$). The intensity of the bicoherence is expressed with different colors. It is clear that the values of $b^2(f_1, f_2)$ at $f_3 = f_1 + f_2 = 9.8$ kHz and $f_2 = \pm 9.8$ kHz are larger than those at other frequencies.

The values of $b^2(f_1, f_2)$ are 0.08–0.12 around the $f_3 = 9.8$ kHz and about 0.01 at other frequencies, which are larger than the noise level given by $1/M = 0.0034$. Therefore, strongly nonlinear coupling is detected in the frequency range of $f_1 + f_2 = 9.8$ kHz, 20 kHz $< f_2 < 80$ kHz, indicating crucially nonlinear interaction between the GAM and ambient turbulence. Figure 4(b) shows the summation of the squared auto-bicoherence $b_s^2(f)$, computed with the same frequency resolution and realizations. The summation is performed for a given frequency. A prominent peak appears at $f_{\text{GAM}} =$

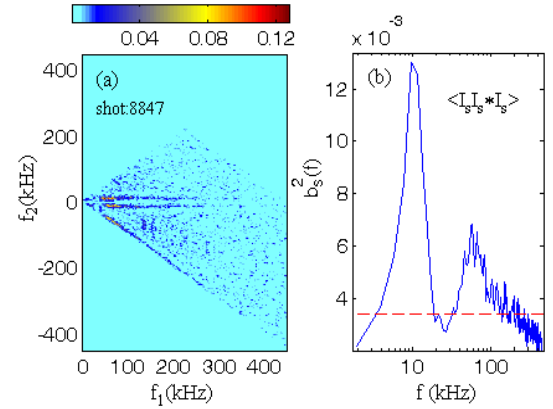


FIG. 4. (a) The squared auto-bicoherence $b^2(f_1, f_2)$ plotted in the $f_1 - f_2$ plane, (b) summed bicoherence $b_s^2(f)$.

The intensity of the squared bicoherence is represented in the color bar. The noise level is 3.4×10^{-3} , indicated by red dotted line.

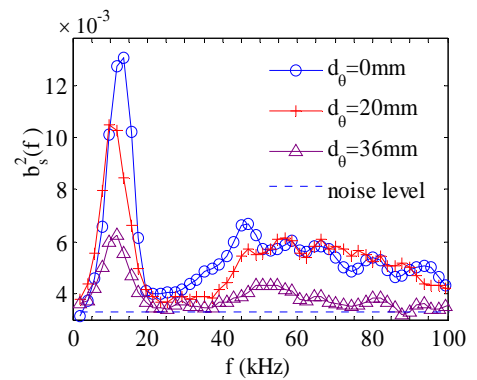


FIG. 5. The summed bicoherence $b_s^2(f)$ of density fluctuation with 3 poloidal separations.

9.8 kHz, implying that strongly nonlinear coupling between the GAM and ambient turbulence is a plausible mechanism for GAM generation. The maximum value is about 0.013, which is obvious over the statistical noise level of 0.0034. The second peak appears at the frequency of 55 kHz, which is related to quasi-mode (QM), whose mechanism is under investigation [29].

The summed bicoherence $b^2(f)$ is the best candidate to characterize the relation between GAM intensity and its spatial scale. The bicoherence spectra have three obvious peaks at the GAM frequency with 3 poloidal separations, as shown in Fig. 5. The peak values at the GAM frequency are 0.013, 0.011, and 0.006, respectively. The coupling intensity decreases with the increase of poloidal separations. A plausible explanation is that the density perturbations with small scales mainly contribute to the generation of GAM density fluctuations through nonlinear three wave coupling. This result is consistent with the inverse cascade [30], which results in the generation of large scale zonal flow through three-wave interaction.

4.3. Relation between the GAM and the HFAT

The envelope analysis is used to identify the modulation interaction between the GAM and the HFAT. The coherency spectra of I_s and its envelope in 200-450 kHz at three different poloidal separations are plotted in Fig. 6(a), where the three curves are for I_{s1} and envelope of I_{s1} , I_{s1} and envelope of I_{s3} with 20 mm poloidal separation, and I_{s1} and envelope of I_{s4} with 36 mm poloidal separation, respectively. The coherency between the original signal I_s and its envelope is high at $f_{\text{GAM}} = 9.8 kHz, indicating that the high frequency component of the density fluctuations strongly correlates with the GAM. The corresponding phase spectra show that the phase shifts between the I_s and its envelopes with different poloidal separations are about 0.9π at the GAM frequency, as shown in Fig. 6(b), which means that the GAM density fluctuations can regulate the HFAT, being similar to the GAM potential modulation. The correlation between the GAM and the high frequency component of density fluctuation is also observed in its temporal evolution. Figure 6(c) shows the filtered signal of I_s in 200-450 kHz and its envelope. The GAM and its envelope with the band-pass of 7.8-11.7 kHz are shown in Fig. 6(d). It is clear that the envelope of band-pass I_s fluctuations delays the GAM by an angle close to π , implying that the envelope modulation of high-frequency density fluctuation is caused by the GAM. This result confirms that the nonlinear coupling between the GAM and the HFAT does exist in density and potential fluctuations.$

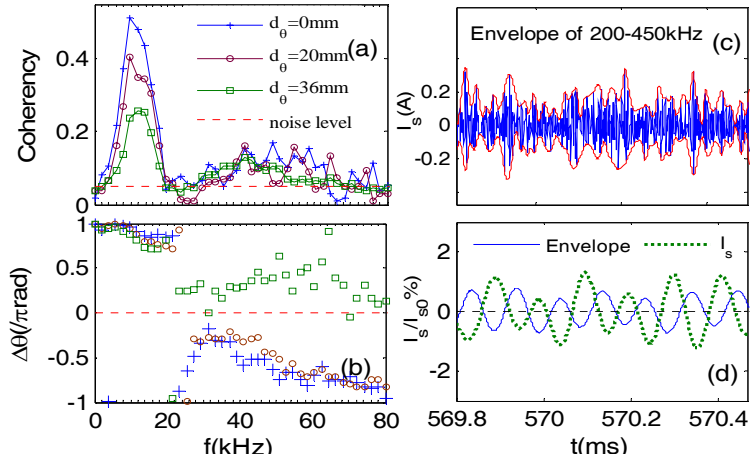


FIG. 6. (a) Coherency spectra of I_s and its envelope in 200-450 kHz at different poloidal separations, (b) the corresponding phase spectra, (c) filtered signal in 200-450 kHz and its envelope indicated by red solid line, (d) temporal evolution of GAM and band-pass filtered envelope (7.8-11.7 kHz) of ambient turbulence.

The corresponding phase spectra show that the phase shifts between the I_s and its envelopes with different poloidal separations are about 0.9π at the GAM frequency, as shown in Fig. 6(b), which means that the GAM density fluctuations can regulate the HFAT, being similar to the GAM potential modulation. The correlation between the GAM and the high frequency component of density fluctuation is also observed in its temporal evolution. Figure 6(c) shows the filtered signal of I_s in 200-450 kHz and its envelope. The GAM and its envelope with the band-pass of 7.8-11.7 kHz are shown in Fig. 6(d). It is clear that the envelope of band-pass I_s fluctuations delays the GAM by an angle close to π , implying that the envelope modulation of high-frequency density fluctuation is caused by the GAM. This result confirms that the nonlinear coupling between the GAM and the HFAT does exist in density and potential fluctuations.

The radial velocity of the GAM is dominated by poloidally electric field (E_θ). Figure 7(a) shows the APS of the E_θ envelope of the HFAT (200-450 kHz). A noticeable peak at $f_{GAM} \sim 9.8$ kHz appears in the spectrum. When the filtered band-pass is the wider, the peak becomes the higher, but it does not change the GAM frequency. The coherency between I_s and the envelope of E_θ is demonstrated in Fig. 7(b). A coherent peak appears at the GAM frequency, obviously over noise level of 0.06. Corresponding phase shift is about 0.9π , as shown in Fig. 7(c), which confirms the modulation interaction between the GAM and the HFAT. This observation has been exhibited in potential fluctuation and is consistent with theoretical prediction. The significant coupling between E_θ and I_s is expected existence in bispectrum.

5. Summary

The density fluctuations with typical GAM frequency of $f_{GAM} \sim 9.8$ kHz are observed at the radius $r/a=0.95$ on the HL-2A tokamak, whose main characteristics have been identified with novel combination of rake and three-step probe arrays. The noticeable peaks at the GAM frequency simultaneously appear in density and potential fluctuations. The mean relative amplitude of the density fluctuation within the FWHM at the GAM frequency is 0.036% near outer midplane, which is consistent with the theoretical prediction ($\sim 0.03\%$). The poloidal and toroidal mode numbers derived from saturation ion currents for two discharges are estimated to be $m = 1.2 \pm 0.4$ and $n = 0.036 \pm 0.039$ as well as $m = -0.73 \pm 0.65$ and $n = 0.035 \pm 0.04$ with two-point correlation technique, respectively. The results are close to the mode numbers of theoretical prediction for the GAM density fluctuations ($m = 0$ or ± 1 and $n = 0$). Meanwhile, the mode numbers for the GAM potential fluctuations are calculated to be $m = 0.23 \pm 0.36$ and $n = 0.04 \pm 0.04$ with the same technique, which are good agreement with theoretic prediction ($m = 0$ and $n = 0$) as well.

The nonlinear coupling between the GAM and ambient turbulence is explored with bispectral analysis. The auto-bicoherence of saturation ion currents shows a noticeable peak under the frequency conditions of $f_{GAM} = f_1 + f_2 = 9.8$ kHz and $20 < f_1 < 250$ kHz, which implies strongly nonlinear interactions between the GAM and ambient turbulence. The summed bicoherence under the fixed frequency $f = f_{GAM}$ has also a peak with the GAM frequency of $f_{GAM} = 9.8$ kHz, suggesting that three-wave interaction is a plausible mechanism to generate the GAM, whose driven energy comes from drift wave turbulence. It is noticed that there is a broad-peak (30-80 kHz) in summed bicoherence, which may be generated from the nonlinear interaction among different frequency components. More examination for the mechanism is our future work.

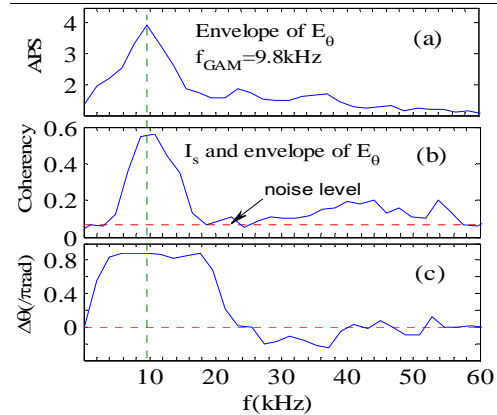


FIG. 7. (a) Auto-power spectrum of the envelope of high frequency component (200-450 kHz) in E_θ , (b) the coherency spectrum of I_s and the envelope of E_θ , (c) corresponding phase shift spectrum.

In addition, the phase shift between density fluctuations and the envelope of high frequency (200-450 kHz) ambient turbulence at the GAM frequency is close to π , which can be considered an indicator for envelope modulation. This observation suggests that the GAM can regulate the ambient turbulence through the envelope modulation.

Acknowledgments

The authors would thank the HL-2A Team for the good operation. This work was supported in part by National Natural Science Foundation of China under Grant Nos. 10675041 and 10775044.

References

- [1] Lin Z. et al., *Science* 281 (1998) 1835.
- [2] Diamond P.H. et al., *Plasma Phys. Control Fusion* 47 (2005) R35.
- [3] Diamond P. H. et al., *Phys. Rev. Lett.* 84 (2000) 4842.
- [4] Xu G. S. et al., *Phys. Rev. Lett.* 91 (2003) 125001.
- [5] Itoh K. et al., *Phys. Plasmas* 12 (2005) 102301.
- [6] McKee G. R. et al., *Phys. Plasmas* 10 (2003), 1712.
- [7] Nagashima Y. et al., *Phys. Rev. Lett.* 95 (2005) 095002.
- [8] Conway C.D. et al., *Plasma Phys. Control Fusion* 47 (2005) 1165.
- [9] Fujisawa A. et al., *Phys. Rev. Lett.* 93 (2004) 165002.
- [10] Fujisawa A. et al., *Nucl. Fusion* 47 (2007) S718.
- [11] Hamada Y. et al., *Nucl. Fusion* 45 (2005) 81.
- [12] Ido T. et al., *Nucl. Fusion* 46 (2006) 512.
- [13] Melnikov A.V. et al., *Plasma Phys. Control Fusion* 48 (2006) S87.
- [14] Shats M. G. And Solomon W. M., *Phys. Rev. Lett.* 88 (2002) 045001.
- [15] Zhao K.J. et al., *Phys. Plasmas* 14 (2007) 122301.
- [16] Lan T. et al., *Phys. Plasmas* 15 (2008) 056105.
- [17] Zhao K.J. et al., *Phys. Rev. Lett.* 96 (2006) 255004.
- [18] Yan L.W. et al., *Nucl. Fusion* 47 (2007) 1673.
- [19] Lan T. et al., *Plasma Phys. Control Fusion* 50 (2008) 045002.
- [20] Gupta D. K. et al., *Phys. Rev. Lett.* 97 (2006) 125002.
- [21] Liu A. D. et al., IAEA-EX/P5-32, 2008.
- [22] Kraemer-Flecken A. et al., *Phys. Rev. Lett.* 97 (2006) 045005.
- [23] Tynan G.R. et al., *Phys. Plasmas* 8 (2001) 2691.
- [24] Nagashima Y. et al., *Plasma Phys. Control Fusion* 49 (2007) 1611.
- [25] Yan L.W. et al., *Rev. Sci. Instru.* 76 (2005) 093506.
- [26] Yan L.W. et al., *Rev. Sci. Instru.* 77 (2006) 113501.
- [27] Cheng J. et al., *Chin.Phys.Lett.* 24 (2007) 3191.
- [28] Conway G. D. et al. *Plasma Phys. Control Fusion* 50 (2008) 055009.
- [29] Zhao K.J. et al., IAEA-EX/P5-34, 2008.
- [30] Xia H. et al., *Phys. Rev. Lett.* 91 (2003) 155001